 doi:10.20944/preprints202205.0097.v1

Article

Design of New Potent and Selective Thiophene-based Kv1.3 Inhibitors and their Potential for Anticancer Activity

Špela Gubič [1], Louise Antonia Hendrickx [2], Xiaoyi Shi [3], Žan Toplak [1], Štefan Možina[1], Kenny M. Van Theemsche[4,5], Ernesto Lopes Pinheiro-Junior [2], Steve Peigneur [2], Alain J. Labro [4,5], Luis A. Pardo [3], Jan Tytgat [2], Tihomir Tomašič [1] and Lucija Peterlin Mašič [1,*]

[1] University of Ljubljana, Faculty of Pharmacy, Aškerčeva 7, 1000 Ljubljana; Slovenia; spela.gubic@ffa.uni-lj.si (Š.G.); zan.toplak@ffa.uni-lj.si (Ž.T.); stefan.mozina@ffa.uni-lj.si (Š.M.); tihomir.tomasic@ffa.uni-lj.si (T.T.); lucija.peterlin@ffa.uni-lj.si (L.P.M)
[2] University of Leuven, Toxicology and Pharmacology, Campus Gasthuisberg, Onderwijs en Navorsing 2, Herestraat 49, PO Box 922, 3000 Leuven, Belgium; louise.hendrickx@kuleuven.be (L.A.H.); ernesto.lopes@kuleuven.be (E.L.P.J); steve.peigneur@kuleuven.be (S.P.); jan.tytgat@kuleuven.be (J.T.)
[3] AG Oncophysiology, Max-Planck Institute for Multidisciplinary Sciences, Hermann-Rein-Str. 3, 37075 Göttingen, Germany; shi@mpinat.mpg.de (X.S.); pardo@mpinat.mpg.de (L.A.P)
[4] University of Antwerp, Laboratory for Molecular, Cellular and Network Excitability, Department of Biomedical Sciences, 2610 Wilrijk, Belgium; Kenny.VanTheemsche@uantwerpen.be (K.M.V.T)
[5] Ghent University, Department of Basic and Applied Medical Sciences, Corneel Heymanslaan 10 (entrance 36), 9000 Ghent, Belgium; alain.labro@ugent.be (A.J.L)
* Correspondence: lucija.peterlin@ffa.uni-lj.si (L.P.M)

Simple Summary: In this article, we describe the discovery of a new class of potent and selective thiophene-based inhibitors of the voltage-gated potassium channel Kv1.3 and their potential to induce apoptosis and inhibit proliferation. The Kv1.3 channel has only recently emerged as a molecular target in cancer therapy. The most potent Kv1.3 inhibitor **44** had an IC_{50} Kv1.3 value of 470 nM (oocytes) and 950 nM (Ltk cells) and appropriate selectivity for other Kv channels. New Kv1.3 inhibitors significantly inhibited proliferation of Panc-1 cells and Kv1.3 inhibitor **4** induced significant apoptosis in tumor spheroids of Colo-357 cells.

Abstract: The voltage-gated potassium channel Kv1.3 has been recognized as a tumor marker and represents a promising new target for the discovery of new anticancer drugs. We designed a novel structural class of Kv1.3 inhibitors through structural optimization of benzamide-based hit compounds and structure-activity relationship studies. The potency, and selectivity of the new Kv1.3 inhibitors were investigated using whole-cell patch- and voltage-clamp experiments. 2D and 3D cell models were used to determine antiproliferative activity. Structural optimization resulted in the most potent and selective Kv1.3 inhibitor **44** in the series with an IC_{50} value of 470 nM in oocytes and 950 nM in Ltk cells. Kv1.3 inhibitor **4** induced significant apoptosis in Colo-357 spheroids, while **14**, **37**, **43**, and **44** significantly inhibited Panc-1 proliferation.

Keywords: Kv1.3; potassium ion channels; antiproliferative activity; apoptosis; anticancer drugs

1. Introduction

The voltage-gated potassium channel Kv1.3 is a transmembrane protein belonging to the Kv1 (Shaker) subfamily, which is the largest subfamily of voltage-gated potassium channels with eight members (Kv1.1-Kv1.8). Kv1.3 is formed by four monomers, each containing six transmembrane segments (S1-S6) [1]. The S5-S6 domain of each monomer assemble to form the K^+ conducting pore that is surrounded by four voltage sensor domains (VSD), each consisting of segments S1 to S4. The VSDs detect depolarization of the membrane and initiate conformational changes that lead to opening of the pore. The selectivity filter in the K^+ conducting pore consists of oxygen cages that mimic the hydration shell of potassium in solution and allow the rapid and selective passage of potassium ions [2–4].

 doi:10.20944/preprints202205.0097.v1

The Kv1.3 channel has only recently emerged as a molecular target in cancer therapy. Cancer cells display mutations enabling extensive proliferation and resistance to apoptosis. Kv1.3 channel activity has been found to be involved in cell proliferation, migration, and invasion, which are among the most important processes in cancer progression. Moreover, overexpression of Kv1.3 enhances tumorigenic processes and promotes tumor progression [5–8]. The use of small-molecule Kv1.3 inhibitors could selectively suppress the proliferation of cancer cells, thus providing a new potential therapeutic approach [9]. Although Kv1.3 has been recognized as a tumor marker in cancer tissues with predominantly higher Kv1.3 expression, a clear pattern of altered Kv1.3 expression in cancer cells compared with healthy cells has not yet been found. The type and stage of disease also influence Kv1.3 expression. Up-regulated Kv1.3 expression was detected in breast, colon, and prostate tumors, in smooth muscle, and skeletal muscle cancers, and in mature neoplastic B cells in chronic lymphocytic leukemia [10]. Due to the aberrant Kv1.3 expression in these cancer cells, the application of Kv1.3 inhibitors would result in a higher level of inhibition in tumors than in normal tissues and target cancer cells for elimination [9].

To date, several small-molecule Kv1.3 inhibitors have been discovered (Figure 1) [11–13]. Originally, Kv1.3 inhibitors were extensively studied to selectively target the proliferation of effector memory T (T_{EM}) cells in the immune system and to develop a new therapy for T-cell–mediated autoimmune and chronic inflammatory diseases [14]. However, none of these compounds have been optimised to have suitable properties for clinical trials. Since Kv1 family channels have high subtype homology, it is very difficult to find a potent isoform-selective Kv1.3 inhibitor [15]. For most of the described compounds, only low or moderate selectivity towards other Kv1.x channels was achieved, preventing subsequent optimization. Cryogenic electron microscopy (cryoEM) was recently used to determine the structures of human Kv1.3 alone and bound to dalazatide, which may aid structure-based design of new inhibitors in the future. To date, the exact binding site for most known Kv1.3 inhibitors has not been experimentally demonstrated, and these new cryoEM structures may help to solve this problem [16,17].

The psoralen derivative PAP-1 (Figure 1, **1**) is the most potent (IC_{50} = 2 nM, L929 cells, manual whole-cell patch clamp) and selective (i.e., 23-fold over Kv1.5) small-molecule Kv1.3 inhibitor known [11]. Benzamide PAC (Figure 1, **2**), which inhibits Kv1.3 with an IC_{50} of 200 nM (CHO cells, $^{86}Rb^+$ efflux), is not selective toward Kv1.x family channels [12]. The antimycobacterial drug clofazimine (Figure 1, **3**) is also a Kv1.3 inhibitor (IC_{50} = 300 nM, Jurkat T cells), inhibiting Kv1.3 with tenfold higher potency than Kv1.1, Kv1.2, Kv1.5 and Kv3.1 [13]. PAP-1 (**1**) at a concentration of 20 µM, and clofazimine (**3**) at a concentration of 1 or 10 µM in combination with the multi-drug resistance (MDR) pump inhibitors (MDRi) cyclosporine H (4 µM) and probenecid (100 µM) induced mild apoptosis in cancer cells (human SAOS2, mouse B16F10 melanoma, and human B-CLL) by specifically inhibiting Kv1.3. Similarly, clofazimine (**3**) induced significant apoptosis in several pancreatic ductal adenocarcinoma (PDAC) cell lines with EC_{50} values in the micromolar range and significantly reduced primary tumor weight in an orthotopic PDAC xenotransplantation model in SCID beige mice [18–20].

 doi:10.20944/preprints202205.0097.v1

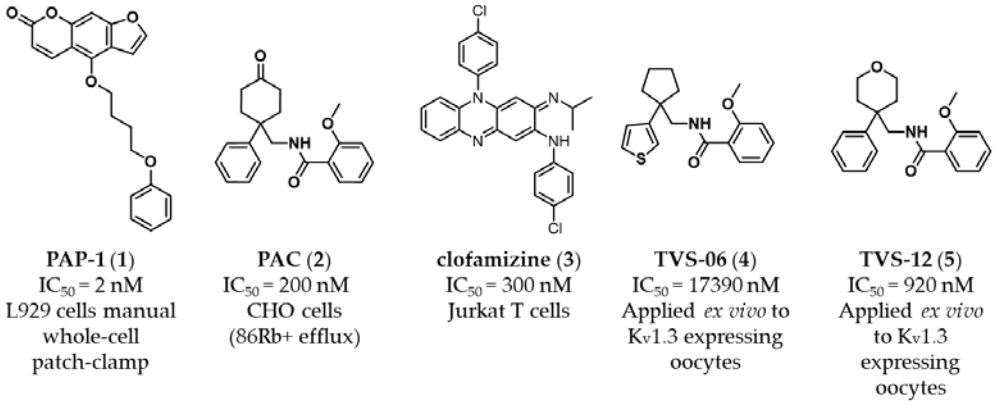

Figure 1. Structures of known representative Kv1.3 inhibitors.

In previous work, we identified two new Kv1.3 inhibitors by virtual screening based on a 3D similarity search using the Kv1.3 inhibitor PAC (**2**, Figure 1) as a query [21]. Hit compound **4**, with an IC_{50} of 17.4 μM was a much weaker Kv1.3 inhibitor than hit compound **5**, with an IC_{50} of 920 nM (applied *ex vivo* in *Xenopus* oocytes expressing Kv1.3). However, Kv1.3 inhibitor **4** exhibited a good selectivity profile and did not affect other Kv1.x family channels or more distantly related channels. In this paper, we describe the optimization of new thiophene-based Kv1.3 inhibitors, their selectivity profile against Kv1.x and some other selected ion channels, and the potential of this new class of Kv1.3 inhibitors for antiproliferative activity in 2D and 3D cell models.

2. Materials and Methods

2.1. Oocyte collection, oocyte injection, drug solutions, electrophysiological recordings, and statistical analysis in Xenopus laevis oocytes

Stage V-VI oocytes were isolated by partial ovariectomy from *Xenopus laevis* frogs (African clawed frogs). Mature female frogs were purchased from CRB Xénopes (Rennes, France) and were housed in the Aquatic Facility (KU Leuven) in compliance with the regulations of the European Union (EU) concerning the welfare of laboratory animals as declared in Directive 2010/63/EU. The use of *Xenopus laevis* was approved by the Animal Ethics Committee of the KU Leuven (Project nr. P186/2019). After anaesthetizing the frogs by a 15-min submersion in 0.1% tricaine methanesulfonate (amino benzoic acid ethyl ester; Merck, Kenilworth, NJ, USA), pH 7.0, the oocytes were collected. The isolated oocytes were then washed with a 1.5 mg/mL collagenase solution for 2 h to remove the follicle layer.

Ion channels (Kv1.x, Kv2.1, Kv4.2, Kv10.1) were expressed in *Xenopus laevis* oocytes, by linearization of the plasmids and subsequent *in vitro* transcription using a commercial T7 or SP6 mMESSAGE mMACHINE transcription kit (Ambion, Carlsbad, California, USA). Defolliculated *Xenopus* oocytes were then injected with 20–50 nL of the cRNA at a concentration of 1 ng/nL using a micro-injector (Drummond Scientific1, Broomall, Pennsylvania, USA). The oocytes were incubated in a solution containing (in mM): NaCl, 96; KCl, 2; $CaCl_2$, 1.8; $MgCl_2$, 2 and HEPES, 5 (pH 7.5), supplemented with 50 mg/L gentamycin sulfate and 90 mg/L theophylline. After *ex vivo* translation, the ion channels are correctly inserted in the cell membrane of the oocytes.

Two-electrode voltage-clamp recordings were performed at room temperature (18–22 °C) using a Geneclamp 500 amplifier (Molecular Devices, San Jose, California, USA) and pClamp data acquisition (Axon Instruments, Union City, California, USA) and using an integrated digital TEVC amplifier controlled by HiClamp, an automated Voltage-Clamp Screening System (Multi Channel Systems MCS GmbH, Reutlingen, Germany). Whole-cell currents from oocytes were recorded 1–4 days after injection. The bath solution composition was ND96 (in mM): NaCl, 96; KCl, 2; $CaCl_2$, 1.8; $MgCl_2$, 2 and HEPES, 5 (pH

 doi:10.20944/preprints202205.0097.v1

7.5). Voltage and current electrodes were filled with a 3 M solution of KCl in H_2O. Resistances of both electrodes were kept between 0.5 and 1.5 MΩ. The elicited Kv1.x, Kv2.1, Kv4.2 and Kv10.1 currents were filtered at 0.5 kHz and sampled at 2 kHz using a four-pole low-pass Bessel filter. Leak subtraction was performed using a P/4 protocol [21].

For the electrophysiological analysis of the compounds, a number of protocols were applied from a holding potential of −90 mV. Currents for Kv1.x, Kv2.1, Kv4.2 and Kv10.1 were evoked by 1 s depolarizing pulses either to 0 mV or to a range of voltage steps between -80 mV and +40 mV. The concentration dependency of all compounds was assessed by measuring the current inhibition in the presence of increasing compound concentrations. To this end, a stock solution of the compounds was prepared in 100% DMSO for the sake of solubility. From this stock solution, adequate dilutions with a maximum of 0.5% DMSO were made for testing. The data of the concentration-response curves were fitted with the Hill equation: $y = 100/\{1 + (IC_{50}/[compound])^h\}$, where y is the amplitude of the compound-induced effect, IC_{50} is the compound concentration at half-maximal efficacy, [compound] is the compound concentration, and h is the Hill coefficient.

All electrophysiological data are presented as means ± S.E.M of n ≥ 3 independent experiments unless otherwise indicated. All data were analyzed using pClamp Clampfit 10.4 (Molecular Devices, Downingtown, Pennsylvania, USA), OriginPro 9 (Originlab, Northampton, Massachusetts, USA), GraphPad Prism 8 software (GraphPad Software, Inc., San Diego, CA, USA) and DataMining (Multi Channel Systems MCS GmbH, Reutlingen, Germany). The Dunnett test and one-way ANOVA were performed to calculate the significance of the induced inhibition compared to the control.

2.2. Cell culture, transfection, drug solutions, electrophysiological recordings, and statistical analysis in Ltk cells

Ltk- cells were cultured in Dulbecco's Modified Eagle Medium (DMEM) supplemented with 10% horse serum and 1% penicillin/streptomycin (Invitrogen, CA, USA). Human $hK_V1.3$ channels were transiently expressed in these Ltk^- cells by transfecting subconfluent 60 x 15 mm cell culture dishes (Corning, NY, USA) with 1-1.5 µg plasmid DNA containing the hKv1.3 sequence (KCNA3) using lipofectamine 2000 (Thermo Fisher Scientific, MA, USA), according to the manufacturer's protocol. The coding sequence of hKv1.3 was cloned in a pEGFP plasmid without removing the stop codon (i.e. eGFP was not transcribed). Therefore, during transfection 0.5 µg of pEGFP plasmid (expressing eGFP) was added as transfection marker Cells were collected 24h post-transfection using a 0.05% trypsin-EDTA solution (Thermo Fisher Scientific, MA, USA) and transferred to the recording chamber mounted on the stage of an inverted Nikon Eclipse TE2000 fluorescence microscope (Nikon, Minato, Japan). The compounds were dissolved in 100% DMSO and stock solutions were stored at -20°C. Before use, the stock concentrations were diluted with extracellular recording solution to appropriate concentrations, making sure that the final DMSO concentration never exceeded 0.1%. As a vehicle control a 0.1% DMSO solution was prepared.

All recordings were conducted at room temperature (20-23°C) in the whole-cell configuration using an axopatch 200b amplifier (Molecular Devices, CA, USA). Applied voltage pulse protocols and current recordings were controlled with pClamp 10 software and digitized using an axon digidata 1440 (Molecular Devices, CA, USA). The cells in the recording chamber were continuously superfused with an extracellular solution (containing in mM): NaCl 145, KCl 4, $MgCl_2$ 1, $CaCl_2$ 1.8, HEPES 10, and glucose 10 (adjusted to pH 7.35 with NaOH). Patch pipettes were pulled from borosilicate glass (World Precision Instruments, FL, USA), using a P-2000 puller (Sutter Instruments, CA, USA), with resistances ranging from 1.5-2 MΩ. These pipettes were backfilled with an intracellular solution (containing in mM): KCl 110, K_2ATP 5, $MgCl_2$ 2, HEPES 10, and K_4BAPTA 5 (adjusted to pH 7.2 with KOH). Junction potentials were zeroed with the filled pipette in the extracellular solution of the recording chamber. A series resistance compensation of 80%

 doi:10.20944/preprints202205.0097.v1

was employed. Recordings were passed through a 5 kHz low-pass filter while being sampled at 10 kHz. $K_V1.3$ currents were elicited by repeated 200 ms pulses from -80 to 40 mV, applied at intervals of 15 s. Only when PAP-1 was applied the protocol was slightly modified: the pulse duration and interval between pulses were increased to 2 s and 30 s respectively. Different concentrations of the compounds were independently added to the recording chamber, in the vicinity of the cell investigated, using a pressurized fast-perfusion system (custom built with electro-fluidic valves from the Lee Company, CT, USA).

The data was analyzed with pClamp 10 software (Molecular Devices, CA, USA), and the dose-response curves shown were made using Sigmaplot 11.0 (Systat software, CA USA). Data was excluded when the estimated voltage error exceeded 5mV after series resistance compensation. Dose-response curves were obtained by plotting y, the normalized current, as a function of compound concentration. Results are expressed as mean ± SEM, with n being the number of cells analyzed. EC_{50} values were determined by fitting the Hill equation to the dose-response curve.

2.3. Cell culture for apoptosis and proliferation assays

Cell lines Panc-1 (ACC 783) and Colo-357 (CVCL_0221) were obtained through the validated collection of the pHioniC consortium (MSC-ITN 813834). Both cell lines were grown in RPMI1640, supplemented with 1 mM sodium pyruvate and 1% Glutamax (all Gibco Thermo-Fisher, Waltham, MA USA) 10%FBS (BioChrom, Berlin, Germany), at 5% CO_2 and 37 °C in a humidified atmosphere.

2.4. Apoptosis and proliferation assays

For cell proliferation assays, cells were seeded at density of 10,000 cells/well in 96-well flat bottom culture plates (Corning, Kaiseslautern, Germany) and proliferation was measured through culture confluency using an IncuCyte device (Sartorius, Göttingen, Germany). Every hour, two phase contrast images per well were acquired, and a confluency mask was generated by training the analysis algorithm using representative images. Every image was then analyzed using the obtained parameters to determine culture confluency. Treatments were then added when cells reached a confluency of ~30% (Panc-1) or ~55% (Colo-357), and proliferation was determined for the following 60 hours. Proliferation is reported as confluency increase with respect to the start of the treatment.

Spheroids were cultured in round bottom ultra-low attachment 96-well plates (Corning). The optimal seeding densities were empirically determined (8000 cells/well for Colo-357 or 10000 cells/well for Panc-1 spheroids. The cells were suspended in 2% Matrigel (Corning), centrifuged at 1000 x*g* for 10 min and the spheroids were allowed to form in the incubator. Once the spheroids formed, the treatments indicated together with 8.9 µM cycloheximide (as apoptosis sensitizer) were added and apoptosis was determined by live imaging in the Incucyte system in real time for approximately 60 hours using as reporter of apoptosis Caspase-3/7 green reagent (Sartorius), which crosses the cell membrane and is cleaved by the activated Caspase-3/7, resulting in the fluorescent staining of nuclear DNA. Apoptosis is presented in the Figure 5E as integrated green fluorescence in the whole spheroid.

2.5. Pharmacophore modeling

Nine inhibitors of $K_V1.3$ with inhibition greater than 75% at a concentration of 10 µM were used for the creation of ten ligand-based pharmacophore models in Ligandscout 4.4 Expert (Inte:Ligand GmbH) [22]. A maximum of 200 conformations were generated for each inhibitor using LigandScout's iCon algorithm [23] and the default "BEST": Max. Number of conformers per molecule: 200; Timeout (s): 600; RMS threshold: 0.8, Energy window: 20.0; Maximum pool size: 4000; Maximum fragment formation time: 30. Pharmacophore models were generated using the following settings for ligand-based pharma-

 doi:10.20944/preprints202205.0097.v1

cophore generation: Scoring function: pharmacophore fit and atom overlap; Pharmacophore type: fused feature pharmacophore; Number of omitted features for merged pharmacophore: 4; partially matching features optional, threshold (%): 10.0; Feature tolerance scale factor: 1.0; Maximum number of result pharmacophores: 10. The creation of exclusion volumes coat around the alignment of the ligands was also enabled for each of the models. All ligands used for pharmacophore modeling were automatically aligned to the generated pharmacophore models. For the interaction analyses and image preparation, best performing pharmacophore model with the best performance was selected based on pharmacophore scoring function.

3. Results

3.1. Design and chemistry

Six different types of cyclopentane-, cyclohexane- and tetrahydropyran-based Kv1.3 inhibitors were designed and synthesized with the aim of increasing potency on Kv1.3, and selectivity against other members of Kv1 family of the hit compounds **4** (TVS-06) and **5** (TVS-12), and to investigate structure-activity relationships (SAR) important for Kv1.3 inhibition. Hit compound **4** (TVS-06) (Figure 2), which contained a scaffold of 3-thiophene, cyclopentane, and 2-methoxybenzamide, was first modified in the aromatic (R^1) or cyclopentane portion of the molecule to yield a new series of cyclopentane or tetrahydrofuran analogs that were screened for Kv1.3 inhibition (Figure 2: Type I compounds). The cyclopentane was replaced by cyclohexane to give new cyclohexane analogs with aromatic R^2 substituents (Figure 2: Type compounds II). In both Type I and II compounds, the 2-methoxybenzamide moiety was retained because it is important for binding to the Kv1.3 channel.

Hit compound **5** with benzene, 2-methoxybenzamide, and tetrahydropyran structural moieties was modified at both aromatic moieties (Figure 2) to give four tetrahydropyran series (Figure 2: Types III-VI). The first strategy was to replace the benzene ring of hit compound **5** with several small substituents to obtain a new series of 2-methoxybenzamide-based compounds (Figure 2: Type III). Based on biological data, an unsubstituted phenyl ring was selected to be included in novel phenyl-based analogs in which modifications were introduced to the 2-methoxybenzamide moiety (Figure 2: Type IV). The unsubstituted phenyl from hit compound **5** was then replaced with various thiophene or thiazole rings (Figure 2: Type V compounds). Finally, new analogs were prepared with the most promising 3-thiophene moiety and with various modifications to the 2-methoxybenzamide moiety (Figure 2: Compounds of Type VI).

Preprints (www.preprints.org) | NOT PEER-REVIEWED | Posted: 9 May 2022 doi:10.20944/preprints202205.0097.v1

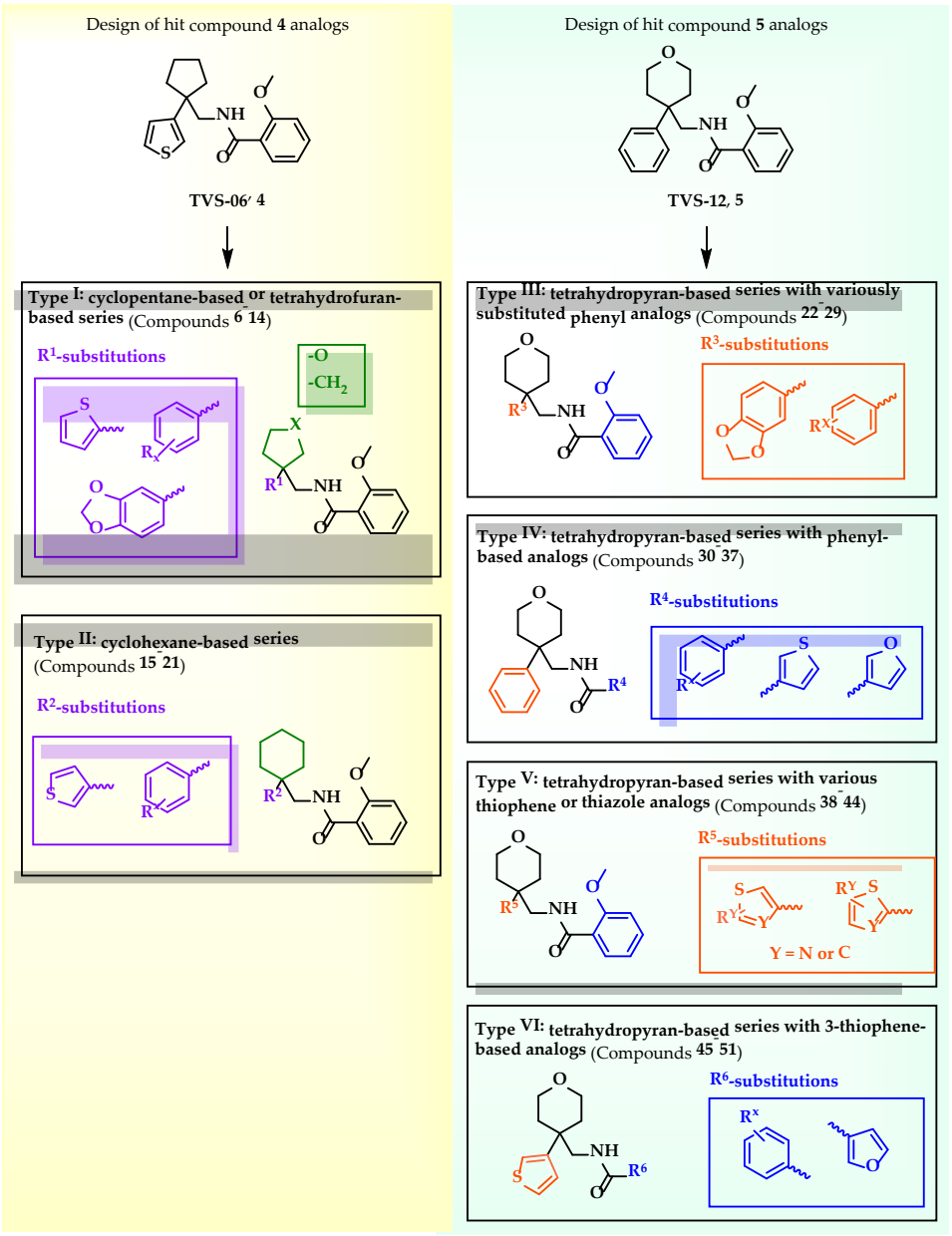

Figure 2. Design of new Kv1.3 inhibitors of structural Types I-VI.

The synthesis of all new analogs is shown in Figures S1-S6. Synthetic procedures, analytical data, chemicals, reagents, and equipment used for organic synthesis and analysis are listed in the Supplementary Materials under the Chemistry section.

3.2. Kv1.3 potencies of structural Type I and Type II compounds

In the Type I series, compound **14** with 2-thiophene and the new tetrahydrofuran ring was the most potent with an IC_{50} value of 0.57 ± 0.36 μM (Table 1), whereas the compounds in the cyclohexane series (Type II compounds **15**-**21**) were inactive (Table 1).

Preprints (www.preprints.org) | NOT PEER-REVIEWED | Posted: 9 May 2022 doi:10.20944/preprints202205.0097.v1

Table 1. Kv1.3 inhibitory activities of new analogues **6-21** from Type I and II series, manually voltage-clamped to determine the percentage of inhibition at 10 μM and the IC_{50}s values determined with manual voltage-clamp on *Xenopus laevis* oocytes.

	Type I 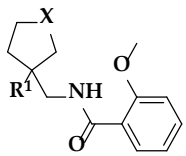				Type II 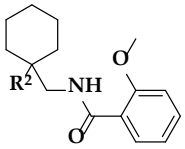	
Compound ID	**R^1**	**X**	**% of Kv1.3 inhibition or IC_{50} [μM]**	**Compound ID**	**R^2**	**% of Kv1.3 inhibition or IC_{50} [μM]**
6	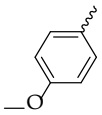	CH_2	<10 %	**15**	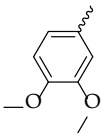	<10 %
7	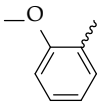	CH_2	<10 %	**16**	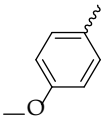	<10 %
8	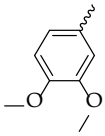	CH_2	<10 %	**17**	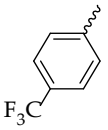	<10 %
9	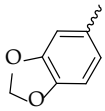	CH_2	<10 %	**18**	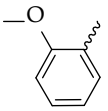	<10%
10		CH_2	<10 %	**19**	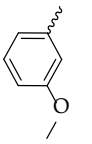	12 ± 2 %
11	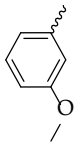	CH_2	18 ± 3 %	**20**	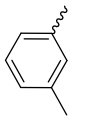	27 ± 2 %
12	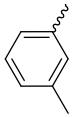	CH_2	16 ± 4 %	**21**		30 ± 8 %
13		CH_2	57 ± 9 %			
14		O	92 ± 4 % 0.57 ± 0.36 μM			

3.3. Kv1.3 potencies of Type III-VI compounds

New tetrahydropyran Kv1.3 inhibitors were designed and synthesized to provide a focused library that was screened for Kv1.3 inhibition (Table 2). The new compounds of Type III **22-29** (Table 2) were modified at the phenyl ring (R^3, Figure 2) of hit compound **5**. The highest percentage of Kv1.3 inhibition of the Type III compounds was achieved with the 3-substituted phenyl analogs (**28-29**), which were less effective compared with hit compound **5**.

Preprints (www.preprints.org) | NOT PEER-REVIEWED | Posted: 9 May 2022 doi:10.20944/preprints202205.0097.v1

The phenyl-based Type IV compounds (**30**-**37**) contained several modifications of the 2-methoxybenzamide moiety of the molecule. The activity of hit compound **5** was maintained with the new 2-methoxy-4-methylbenzamide (**36**) and 5-fluoro-2-methoxybenzamide (**37**) analogs (Table 2), which exhibited around two times higher IC_{50} values than **5**.

In the Type V series, the benzene ring of hit compound **5** was replaced by several thiophene or thiazole moieties (Figure 2, **38**-**44**) to obtain a suitable moiety that would give better selectivity and potency compared with the benzene ring of hit compound **5**. Two potent Type V inhibitors were obtained by using 2-thiophene (**43**) or 3-thiophene (**44**) moieties. The 2-thiophene analog **43** had a nanomolar IC_{50} value of 0.59 ± 0.15 μM and the most potent Type V compound was the 3-thiophene analog **44** with an IC_{50} value of 0.47 ± 0.02 μM.

Because Type V compound **44** had a lower IC_{50} value for Kv1.3 compared to hit compound **5**, the 3-thiophene moiety was determined to be the most promising bioisosteric replacement for the benzene ring and was incorporated into a new Type VI 3-thiophene-based analogs **45**-**50** (Table 2) with modifications of the 2-methoxybenzamide part of the molecule (Figure 2). The most potent Type VI compound was the 2-methoxy-4-methylbenzamide analog **51**, which had an IC_{50} value of 2.92 ± 0.12 μM (Table 2).

Table 2. Structures and Kv1.3 inhibitory potencies of the designed and synthesized Type IV-VI analogues **22**-**51**, manually voltage-clamped to determine the percentage of inhibition at 10 μM and the IC_{50}s values determined with manual voltage-clamp or HiClamp* on oocytes.

	Type III			Type V	
	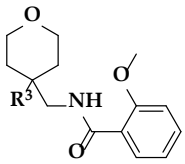			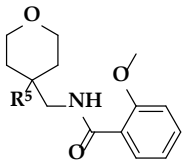	
Compound ID	**R^3**	**% of Kv1.3 inhibition or IC_{50} [μM]**	**Compound ID**	**R^5**	**% of Kv1.3 inhibition or IC_{50} [μM]**
22	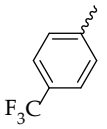	<10 %	**38**	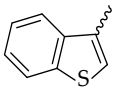	<10 %
23	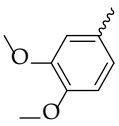	<10 %	**39**	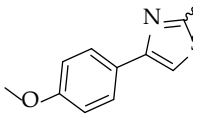	<10 %
24	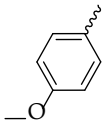	59 ± 5 %	**40**	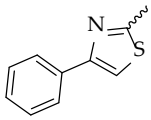	<10 %
25	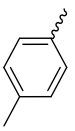	52 ± 8 %	**41**		41 ± 10 %
26	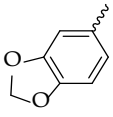	60 ± 9 %	**42**		54 ± 10 %

Preprints (www.preprints.org) | NOT PEER-REVIEWED | Posted: 9 May 2022 doi:10.20944/preprints202205.0097.v1

27	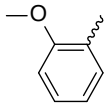	78 ± 4 %	**43**		92 ± 1 % 0.59 ± 0.15 µM
28	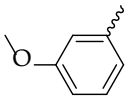	88 ± 4 % 5.75 ± 1.11 µM	**44**		96 ± 1 % 0.47 ± 0.02 µM
29	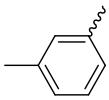	87 ± 4 % 4.30 ± 0.33 µM			

Type IV

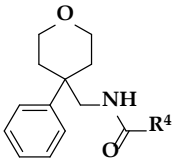

Type VI

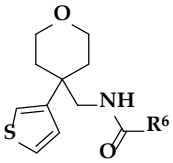

Compound ID	R^4	% of Kv1.3 inhibition or IC_{50} [µM]	Compound ID	R^6	% of Kv1.3 inhibition or IC_{50} [µM]
30	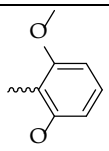	<10 %	**45**	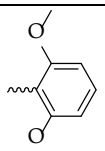	<10%
31	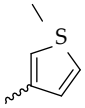	11 ± 4 %	**46**	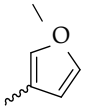	21 ± 6 %
32		27 ± 6 %	**47**	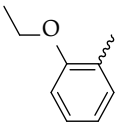	35 ± 8 %
33	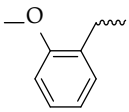	38 ± 5 %	**48**	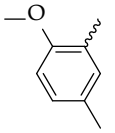	42 ± 6 %
34	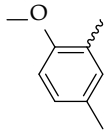	47 ± 1 %	**49**	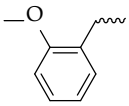	43 ± 1 %
35	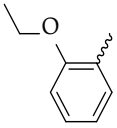	74 ± 9 %	**50**	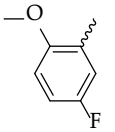	47 ± 9 %
36	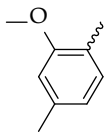	89 ± 4 % 1.65 ± 0.38 µM*	**51**	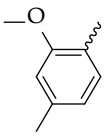	82 ± 1 % 2.92 ± 0.12 µM*
37	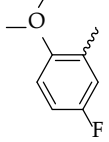	94 ± 1 % 1.97 ± 0.14 µM*			

3.4. Selectivity and IC_{50} determinations of the most potent Kv1.3 inhibitors

The most potent compounds from Tables 1 and 2 (**14**, **37**, **43** and **44**) and the reference compound PAP-1 (**1**) were tested for Kv1.3 inhibition with an additional independent

Preprints (www.preprints.org) | NOT PEER-REVIEWED | Posted: 9 May 2022 doi:10.20944/preprints202205.0097.v1

method of manual patch-clamp procedures on human Ltk cells. The aim was to demonstrate the inhibition of Kv1.3 also in a human cell line and to have a direct comparison with the positive control PAP-1 (**1**), which was previously tested in L929 cells and human T-cells (IC_{50} of 2 nM**)** [11]. Interestingly, the reference compound PAP-1 (**1**) had an IC_{50} value of 780 nM (manual voltage clamp on oocytes) and 370 nM (manual patch clamp on Ltk cells), which is a much lower potency compared to literature data (IC_{50} of 2 nM, L929 cells, manual whole-cell patch-clamp). The best compound of Types I- VI had comparable potency on oocytes (manual voltage-clamp) and human Ltk cells (manual patch-clamp) of 470 nM and 950 nM, respectively.

Table 3. Comparison of Kv1.3 IC_{50} values for compounds **14**, **37**, **43**, **44**, and PAP-1 (**1**) obtained with HiClamp and manual voltage-clamp on *Xenopus laevis* oocytes (Tables 1 and 2) and with manual patch-clamp on human Ltk cell-line.

Compound ID	IC_{50} (manual voltage -clamp oocytes) [µM]	IC_{50} (HiClamp oocytes) [µM]	IC_{50} (manual patch-clamp Ltk) [µM]
PAP-1 (1)	0.78 ± 0.01	2.67 ± 0.30	0.37 ± 0.02
14	0.57 ± 0.36	1.03 ± 0.03	1.33 ± 0.20
37	3.96 ± 0.47	1.97 ± 0.14	1.35 ± 0.04
43	0.59 ± 0.15	1.20 ± 0.02	1.02 ± 0.07
44	0.47 ± 0.02	1.99 ± 0.61	0.95 ± 0.24

The aim of new potent Kv1.3 inhibitors is sufficient selectivity against other voltage-gated potassium channels. Therefore Kv1.3 inhibitors **14**, **37**, **43**, and **44** were screened against a panel of voltage-dependent channels (Figure 3) using the *Xenopus laevis* heterologous expression system together with the reference compound PAP-1 (**1**). These channels were selected based on their importance in cardiac physiology and their structural similarity to Kv1.3. PAP-1 (**1**) was tested at a concentration of 10 µM (Figure 3) and showed no significant effects on the channels Kv1.1, Kv1.2, Kv1.4, Kv1.5, Kv1.6, Kv2.1, Kv4.2, and Kv10.1 in *Xenopus laevis* oocytes. Compounds **14**, **37**, **43**, and **44** were screened at the concentration of their IC_{50} values for Kv1.3. IC_{50} values for other Kv channels were determined for the compounds that showed significant activity on other potassium channels compared with Kv1.3 (Table 4).

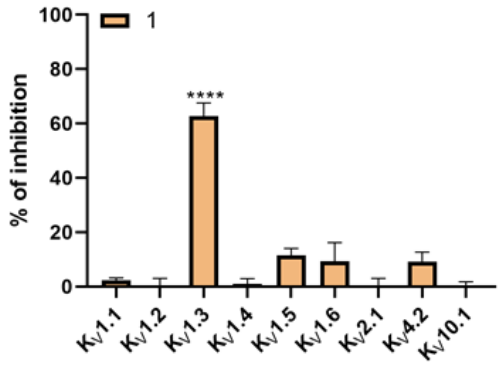

Figure 3. Selectivity determination of PAP-1 (**1**) screened at a concentration of 10 µM (HiClamp *Xenopus laevis* heterologous expression system) on a panel of ion channels. (****p<0.0001, Mean ± S.E.M, N=3-12).

At a concentration of its IC_{50} value (IC_{50} = 1.99 ± 0.61 µM, Table 4) for Kv1.3, compound **44** with the 3-thiophene ring showed no significant effects on channels Kv1.1, Kv1.2, Kv1.5, Kv1.6, Kv2.1 and Kv10.1. However, it induced approximately 16% inhibition of Kv1.4 at this concentration, which is why the IC_{50} value was determined for Kv1.4 (8.48 ± 2.21 µM,

Preprints (www.preprints.org) | NOT PEER-REVIEWED | Posted: 9 May 2022 doi:10.20944/preprints202205.0097.v1

Table 4). Compound **44** showed the most appropriate selectivity profile compared to the other new Kv1.3 inhibitors **14**, **37**, and **43**.

At a concentration of their IC_{50} values for Kv1.3, **14** and **43**, based on 2-thiophene scaffolds, showed significant effects on Kv1.1, Kv1.2, Kv1.5, and Kv1.6 (Figure 4), so IC_{50} values were determined for these channels. Compound **14** (IC_{50} = 1.03 ± 0.03 μM for Kv1.3, Table 4) very potently inhibited Kv1.1 (IC_{50} = 0.71 ± 0.26 μM, Table 4) and Kv1.6 currents (IC_{50} = 0.43 ± 0.02 μM, Table 4). Similarly, **43** (IC_{50} = 1.20 ± 0.02 μM for Kv1.3, Table 4) proved to be an even more potent inhibitor of Kv1.1 (IC_{50} = 0.56 ± 0.12 μM, Table 4) and Kv1.6 (IC_{50} = 0.83 ± 0.01 μM, Table 4) channels.

Compound **37**, containing a phenyl ring, at the concentration of the IC_{50} for Kv1.3 (IC_{50} = 1.97 ± 0.14 μM, Table 4) significantly inhibited the currents of Kv1.1, Kv1.2, Kv1.5, and Kv1.6 (Table 4).

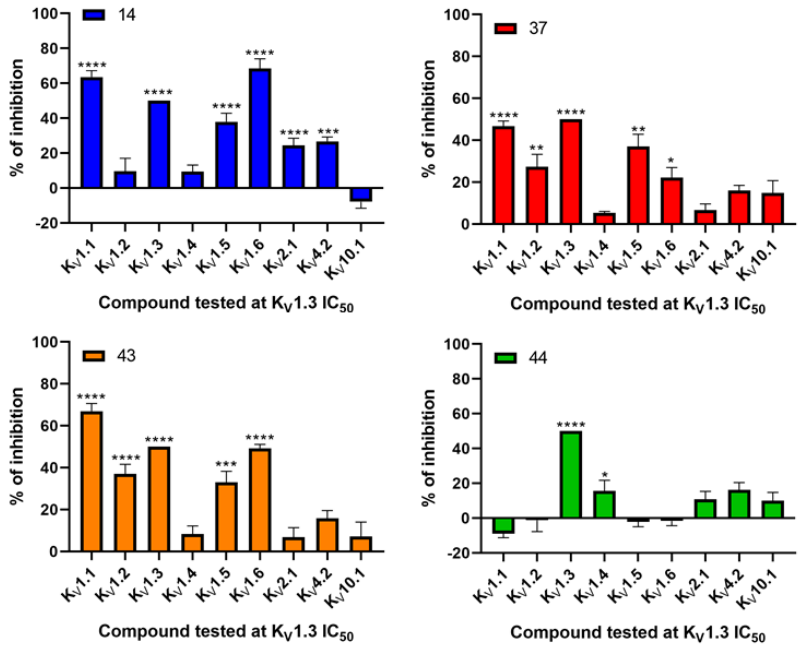

Figure 4. Selectivity determination of **14**, **37**, **43**, and **44** screened at a concentration of their IC_{50} values for Kv1.3 on a panel of ion channels. ****p<0.0001, ***p< 0.001, **p<0.01 *p<0.05, Mean ± S.E.M, N=3-12).

Table 4. IC_{50}s values [μM] for analogues **PAP-1**, **14**, **37**, **43**, and **44** on relevant voltage-gated ion channels. IC_{50} values were determined with HiClamp *Xenopus laevis* heterologous expression system for analogues which showed significant inhibition on the tested ion channels in Figure 4. The NA means that the analogue did not show significant inhibition on the tested ion channel and hence no IC_{50} was determined.

	PAP-1 (1)	14	37	43	44
Kv1.1	NA	0.71 ± 0.26	1.76 ± 0.40	0.56 ± 0.12	NA
Kv1.2	NA	4.00 ± 0.20	2.34 ± 0.26	2.76 ± 0.56	NA
Kv1.3	2.67 ± 0.30	1.03 ± 0.03	1.97 ± 0.14	1.20 ± 0.02	1.99 ± 0.61
Kv1.4	NA	NA	NA	NA	8.48 ± 2.21
Kv1.5	NA	2.07 ± 0.13	8.64 ± 0.03	4.33 ± 0.01	NA
Kv1.6	NA	0.43 ± 0.02	4.33 ± 1.21	0.83 ± 0.01	NA
Kv2.1	NA	6.45 ± 0.42	NA	NA	NA
Kv4.2	NA	2.41 ± 0.88	NA	NA	NA
Kv10.1	NA	NA	NA	NA	NA

 doi:10.20944/preprints202205.0097.v1

3.5. Effects on the growth of cell lines in 2D cell culture

Kv1.3 is associated with the control of cell proliferation in various cancer cell types. Therefore, we investigated the effects of compounds **14**, **37**, **43** and **44** on the proliferation of two pancreatic cancer cell lines, Panc-1 and Colo-357, which have been reported to overexpress Kv1.3 [19]. The compounds were tested at a concentration of 100 μM, which is the maximal concentration we can achieve while maintaining a low concentration of vehicle (1% DMSO, which was also added to the control). Proliferation was determined as confluence of the culture using live cell imaging over a 72 hour period. For Panc-1 cells (Figure 5A and 5C), compound **44** caused moderate growth inhibition, whereas **14**, **43**, and especially **37** caused strong inhibition. However, the growth of Colo-357 cells (Figure 5B and 5D) was not significantly affected by any of the compounds.

3.6. Effects on the growth of cell lines in 3D cell culture.

To test the ability of the compounds to inhibit tumour progression in a more predictive system, we performed experiments on tumour spheroids of the pancreatic cancer cell lines used for 2D culture. In Panc-1 spheroids (Figure 5E), the compounds that effectively reduced proliferation in 2D culture (**14**, **37**, **43**, and **44**) did not induce detectable levels of apoptosis, whereas the reference compound PAP-1 did. In Colo-357 cell spheroids, significant induction of apoptosis was observed in the presence of the hit compound **4** (Figure 5F). None of the other compounds tested differed significantly from control. The degree of apoptosis induction was dose-dependent, although we could not use concentrations higher than 100 μM and therefore cannot determine the IC_{50} for induction of apoptosis. The level of apoptosis achieved by 100 μM of hit compound **4** was similar to that achieved by 50 μM PAP -1 (**1**).

4. Discussion

With the structure-activity relationship studies of novel structural classes Kv1.3 inhibitors, we identified structural parts that are important for Kv1.3 inhibition. With structural optimization of hit compounds **4** and **5** we developed new Kv1.3 inhibitors (e.g. **14**, **43**, and **44)** with improved potency compared to hit compounds. To explain the structural requirements for Kv1.3 inhibition, we created a pharmacophore model of the new Kv1.3 inhibitors in Ligandscout 4.4 Expert (Inte:Ligand GmbH), using inhibitors that achieved Kv1.3 inhibition greater than 75% at a concentration of 10 μM. The ligand-based pharmacophore model (Figure 6) is presented with the structure of the most potent Kv1.3 inhibitor **44**. Structural elements in the most potent analogs that were required for high-affinity interaction with Kv1.3 were amide bond (hydrogen bond acceptor, HBA, hydrogen bond donor, HBD), two aromatic features, oxygen in the 2-methoxy group as HBA, and oxygen in the rings of tetrahydrofuran (Type I) or tetrahydropyran (Type III-VI) rings as HBA. 2-Methoxybenzamide was present in the first aromatic feature (Types I, III and V) of the most potent molecules, but some alternatives such as 2-methoxy-4-methylbenzamide (Type IV, **36** and Type VI, **51**) and 5-fluoro-2-methoxybenzamide (Type IV, **37**) were also tolerated. The second aromatic feature of most potent inhibitors included 3-substituted (Type III, **28** and **29**) or unsubstituted benzene (Type IV, **36**, **37**), unsubstituted 2-thiophene (Type I, **14** and Type V, **43**) or unsubstituted 3-thiophene (Type V, **44** and Type VI, **51**).

Several known small molecule Kv1.3 inhibitors lack selectivity for Kv1.3 over the closely related Kv1.x family channels, which have high subtype homology. The lack of selectivity for Kv1.5 raises many concerns regarding potential acute cardiac toxicity. Obtaining a selective small molecule inhibitor remains a major challenge, and often the lack of selectivity prevents subsequent optimization. Based on literature data, PAP-1 (Figure 1, **1**) is selective toward Kv1 channels, whereas it has the lowest selectivity toward the Kv1.5 channel (i.e., 23-fold over Kv1.5). We included into our testing also the reference compound PAP-1 to have a direct comparison of potency and selectivity with newly de-

Preprints (www.preprints.org) | NOT PEER-REVIEWED | Posted: 9 May 2022 doi:10.20944/preprints202205.0097.v1

signed compounds. We determined IC_{50} values for PAP-1 using three independent methods: manual voltage clamp on oocytes (IC_{50} = 0.78 ± 0.01 µM), HiClamp system on oocytes (IC_{50} = 2.67 ± 0.30 µM), and manual patch clamp on Ltk cells (IC_{50} = 0.37 ± 0.02 µM). Surprisingly, the IC_{50} values determined for PAP-1 were approximately 185- to 1335-fold higher than the literature IC_{50} value of 2 nM (L929 cells, manual whole-cell patch-clamp) [25]. Regarding selectivity, the PAP-1 tested at a concentration of 10 µM showed no significant effects on channels Kv1.1, Kv1.2, Kv1.4, Kv1.5, Kv1.6, Kv2.1, Kv4.2, and Kv10.1 using HiClamp system on oocytes.

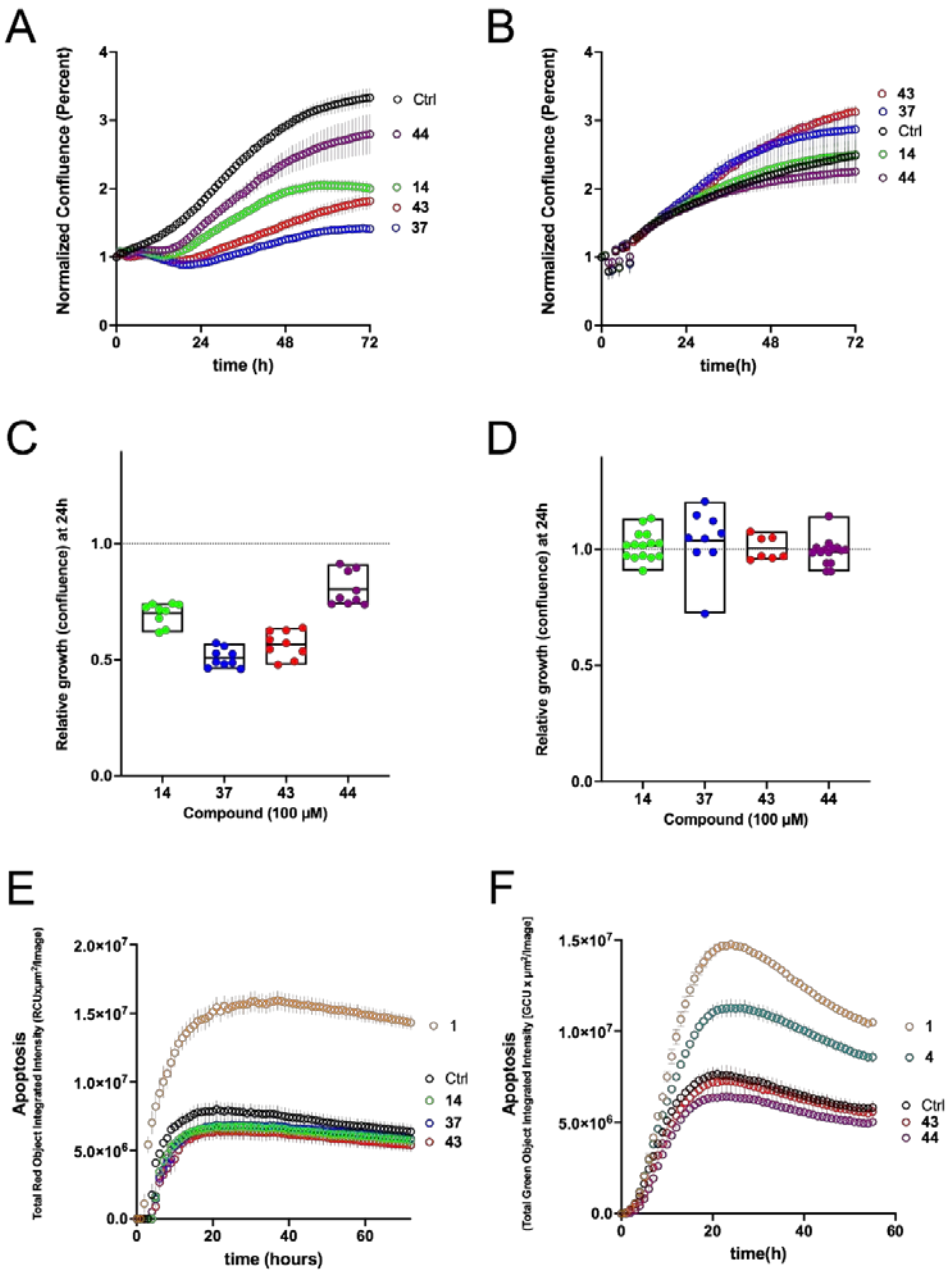

Figure 5. Effects on pancreatic cancer cell lines in 2D and 3D cell cultures. (A) Growth curves (culture confluence measured through phase contrast imaging) of Panc-1 cells in the presence of the indicated compounds (100 µM) or the vehicle (DMSO, black symbols). Mean ± S.E.M, N=9. (B) The equivalent experiment on Colo-357 cells revealed that the growth inhibition was cell-type specific. Mean ± S.E.M, N=15. The inhibition 24 h after the start of treatment is quantified in (C) and (D) for the data presented in (A) and (B) respectively. (E) Apoptosis measured as caspase 3/7 activity on Panc-1 tumor spheroids in the presence of the indicated compounds. (F) Apoptosis in Colo-357 tumor spheroids ($p<0.001$, Mean ± S.E.M, N=4).

Preprints (www.preprints.org) | NOT PEER-REVIEWED | Posted: 9 May 2022 doi:10.20944/preprints202205.0097.v1

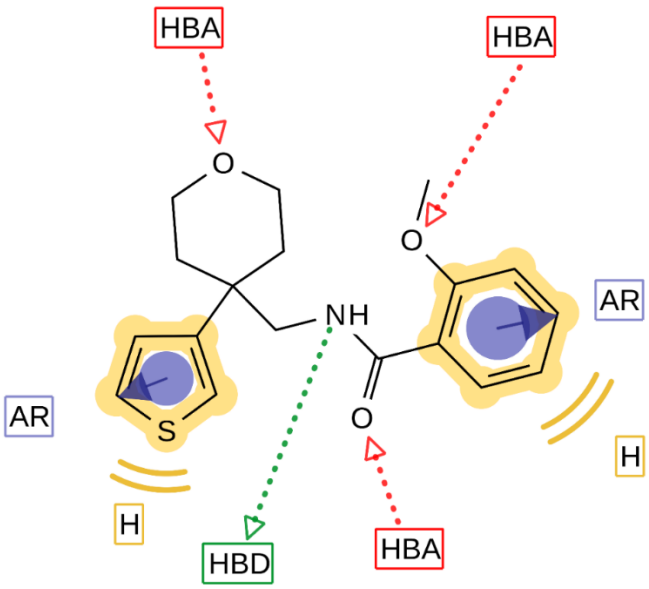

Figure 6. Pharmacophore model of new Kv1.3 inhibitors. The model was prepared in the Ligandscout 4.4 Expert (Inte:Ligand GmbH) [22,24] using molecules with inhibition of Kv1.3 higher than 75 % at 10 μM concentration. Pharmacophore features represent: hydrophobic interactions, yellow spheres; aromatic interactions, blue discs; hydrogen bond donor, green arrow; hydrogen bond acceptors, red spheres. Pharmacophore model shows most important features of Kv1.3 inhibitors with most potent compound **44** aligned to pharmacophore model.

Our aim was to design novel potent and selective Kv1.3 inhibitors based on previously determined hit compounds **4** and **5**. Based on selectivity data for hit compounds **4** and **5**, we hypothesized that the 3-thiophene scaffold and/or the 2-methoxybenzamide moiety together might be responsible for the high selectivity of hit compound **4**. To test this hypothesis, we designed six types of novel analogs (Types I-VI) that incorporated 3-thiophene (Types V and VI), 2-thiophene (Types I and V), or benzene (Types III or IV) as scaffolds in the amine portion of the molecules. Compounds **43** (Type I) and **44** (Type V) had very similar affinity for Kv1.3 (IC_{50} = 0.59 ± 0.15 μM and 0.47 ± 0.02 μM, respectively), but interestingly, the 2- or 3-thiophene position leads to a completely different selectivity profile. Among the new Kv1.3 inhibitors, **44** (type V) with 3-thiophene scaffold and 2-methoxybenzamide moiety showed the best selectivity profile showing no significant inhibition of Kv1.x channels except it inhibited Kv1.4 with IC_{50} value of 8.48 ± 2.21 μM. In contrast, inhibitors **14**, and **43** with 2-thiophene scaffold and 2-methoxy benzamide moiety lacked selectivity toward Kv1.1, Kv1.2, Kv1.5, and Kv1.6. It appears that both the 3-thiophene scaffold and the 2-methoxybenzamide moiety are responsible for the high selectivity of hit compound **4** and the novel benzamide analog **44**, but the new structural elements of tetrahydropyran (**37**, **43** and **44**) and tetrahydrofuran (**14**) allow higher potency for Kv1.3.

Kv1.3 activity is required for cell proliferation, migration, and invasion, which are very important events in cancer progression [9]. To date, there are several lines of evidence that cell-permeable inhibitors of Kv1.3, PAP-1 (**1**) and clofazimine (**3**), specifically target Kv1.3 to mediate apoptosis. However, PAP-1-based mitochondria-targeted derivatives (PAPTP and PCARBTP) bound to the lipophilic triphenylphosphonium cation (TPP) were found to be very effective in several cancer models, including pancreatic ductal adenocarcinoma, melanoma, and glioblastoma [26,27]. PAPTP and PCARBTP were able to decrease the cell survival with EC_{50} of approximately 3 and 6 μM in Panc-1 cell line. The decrease in MTS levels when 10 μM PAPTP or PCARBTP was used was due to apoptosis of Panc-1, while clofazimine only induced cell death of less than 30% even at a concentration of 20 μM. On the other hand, cell death of Colo-357 was achieved only after treatment with high

 doi:10.20944/preprints202205.0097.v1

concentrations of PAPTP, PCARBTP, and clofazimine (EC_{50}s of 3.7, 2, and 1.5 μM, respectively) [27].

We tested the ability of our new potent Kv1.3 inhibitors to inhibit the proliferation of two Kv1.3-expressing PDAC cell lines, Colo-357 (metastatic) and Panc-1 (from the pancreatic duct). Growth of Panc-1 cells was inhibited by Kv1.3 inhibitors **14**, **37**, **43**, and **44**, with **37** in particular causing strong inhibition. Colo-357 growth was unaffected in the presence of these compounds. In Colo-357 tumor spheroids, starting hit compound **4** induced a significant amount of apoptosis, and the degree of apoptosis achieved by 100 μM of **4** was similar to that achieved by 50 μM PAP-1 (**1**). All compounds were ineffective as apoptosis inducers in Panc-1 tumor spheroids, whereas PAP-1 was able to induce significant apoptosis (not shown). Based on our efficacy data in PDAC cell lines and Colo-357 tumor spheroids, we hypothesize that inhibition of mitochondrial Kv1.3 ion channels is required for significant anticancer activity, as previously demonstrated with PAP-1-based mitochondrial Kv1.3 inhibitors (PAPTP and PCARBTP). This suggests the potential to develop new mitochondrial Kv1.3 inhibitors by adding TPP moiety to our potent and selective thiophene-based Kv1.3 inhibitors.

5. Conclusions

To discover a novel structural class of Kv1.3 inhibitors overexpressed in many different tumour types, we used a structural optimization approach and successfully prepared novel potent and selective thiophene-based Kv1.3 inhibitors. We identified the potent and appropriately selective nanomolar Kv1.3 inhibitor **44**, which contains 3-thiophene and tetrahydropyran scaffolds. We demonstrated inhibition of Panc-1 cancer cell line proliferation by the new Kv1.3 inhibitors. Hit compound **4** induced significant apoptosis in Colo-357 tumour spheroids, and the extent of apoptosis achieved by 100 μM of **4** was comparable to that achieved by 50 μM PAP-1 (**1**). Based on the efficacy data in PDAC cell lines and Colo-357 tumour spheroids, we can assume that newly developed Kv1.3 inhibitors do not reach the mitochondrial Kv1.3 channels required for induction of apoptosis. There is an opportunity to further develop the new structural class of potent and selective Kv1.3 inhibitors into mitochondrial Kv1.3 inhibitors by adding mitochondrial targeting moieties.

Supplementary Materials: The following are available online at www.mdpi.com/xxx/s1, Table S1:, Table S2:, Table S3:, Chemistry: analytical procedures description and NMR spectrums.

Author Contributions: For research articles with several authors, a short paragraph specifying their individual contributions must be provided. The following statements should be used "Conceptualization, Š.G., S.P., J.T., T.T., L.A.P. and L.P.M.; methodology, J.T., S.P., T.T., L.A.P. and L.P.M.; formal analysis, Š.G., L.A.H., Š.M., M.N., E.L.P-J, S.P. and L.A.P.; investigation, Š.G., L.A.H., X.S., K.M.V.T, T.T. and L.A.P.; data curation, Š.G., L.A.H., X.S.,S.T., K.M.V.T, T.T. and L.A.P.; writing—original draft preparation, Š.G., J.T., T.T., L.A.P. and L.P.M.; writing—review and editing, J.T., K.M.V.T, A.J.L.,T.T., L.A.P. and L.P.M.; supervision, S.P., J.T., A.J.L., T.T., L.A.P. and L.P.M.; project administration, J.T., T.T., L.A.P. and L.P.M.; funding acquisition, J.T., L.A.P. and L.P.M.. All authors have read and agreed to the published version of the manuscript.

Funding: This research was funded by Slovenian Research Agency (ARRS) grant numbers J1-9192, N1-0098, P1-0245 and CELSA project. The work has also received funding from the Max-Planck Society and from the European Union through Horizon 2020 research and innovation programme under the Marie Skłodowska-Curie grant agreement No. 813834-PHIONIC-H2020-MSCA-ITN-2018. This study was supported by grants GOE7120N, GOC2319N, and GOA4919N from the F.W.O. Vlaanderen, awarded to J.T. and S.P. was supported by KU Leuven funding (PDM/19/164) and F.W.O. Vlaanderen grant 12W7822N.

Data Availability Statement: The data presented in this study are available on request from the corresponding author.

Acknowledgments: We thank OpenEye Scientific Software, Santa Fe, NM, USA, for free academic licenses for the use of their software. L.A.P. thanks the expert technical assistance of V. Díaz.

Conflicts of Interest: The funders had no role in the design of the study; in the collection, analyses, or interpretation of data; in the writing of the manuscript, or in the decision to publish the results.

References

1. Serrano-Albarrás, A.; Estadella, I.; Cirera-Rocosa, S.; Navarro-Pérez, M.; Felipe, A. Kv1.3: A Multifunctional Channel with Many Pathological Implications. *Expert Opin. Ther. Targets* **2018**, *22*, 101–105, doi:10.1080/14728222.2017.1420170.
2. Rudy, B.; Maffie, J.; Amarillo, Y.; Clark, B.; Goldberg, E.M.; Jeong, H.-Y.; Kruglikov, I.; Kwon, E.; Nadal, M.; Zagha, E. Voltage Gated Potassium Channels: Structure and Function of Kv1 to Kv9 Subfamilies. In *Encyclopedia of Neuroscience*; Elsevier, 2009; pp. 397–425 ISBN 978-0-08-045046-9.
3. Kuang, Q.; Purhonen, P.; Hebert, H. Structure of Potassium Channels. *Cell. Mol. Life Sci.* **2015**, *72*, 3677–3693, doi:10.1007/s00018-015-1948-5.
4. Long, S.B.; Campbell, E.B.; MacKinnon, R. Crystal Structure of a Mammalian Voltage-Dependent Shaker Family Kþ Channel. **2005**, *309*, 8.
5. Pardo, L.A. Voltage-Gated Potassium Channels in Cell Proliferation. *Physiol. Bethesda Md* **2004**, *19*, 285–292, doi:10.1152/physiol.00011.2004.
6. Serrano-Novillo, C.; Capera, J.; Colomer-Molera, M.; Condom, E.; Ferreres, J.; Felipe, A. Implication of Voltage-Gated Potassium Channels in Neoplastic Cell Proliferation. *Cancers* **2019**, *11*, 287, doi:10.3390/cancers11030287.
7. Comes, N.; Serrano-Albarrás, A.; Capera, J.; Serrano-Novillo, C.; Condom, E.; Ramón y Cajal, S.; Ferreres, J.C.; Felipe, A. Involvement of Potassium Channels in the Progression of Cancer to a More Malignant Phenotype. *Biochim. Biophys. Acta BBA - Biomembr.* **2015**, *1848*, 2477–2492, doi:10.1016/j.bbamem.2014.12.008.
8. Pérez-García, M.T.; Cidad, P.; López-López, J.R. The Secret Life of Ion Channels: Kv1.3 Potassium Channels and Proliferation. *Am. J. Physiol.-Cell Physiol.* **2018**, *314*, C27–C42, doi:10.1152/ajpcell.00136.2017.
9. Teisseyre, A.; Palko-Labuz, A.; Sroda-Pomianek, K.; Michalak, K. Voltage-Gated Potassium Channel Kv1.3 as a Target in Therapy of Cancer. *Front. Oncol.* **2019**, *9*, 933, doi:10.3389/fonc.2019.00933.
10. Comes, N.; Bielanska, J.; Vallejo-Gracia, A.; Serrano-Albarrás, A.; Marruecos, L.; Gómez, D.; Soler, C.; Condom, E.; Ramón y Cajal, S.; Hernández-Losa, J.; et al. The Voltage-Dependent K+ Channels Kv1.3 and Kv1.5 in Human Cancer. *Front. Physiol.* **2013**, *4*, doi:10.3389/fphys.2013.00283.
11. Schmitz, A.; Sankaranarayanan, A.; Azam, P.; Schmidt-Lassen, K.; Homerick, D.; Hänsel, W.; Wulff, H. Design of PAP-1, a Selective Small Molecule Kv1.3 Blocker, for the Suppression of Effector Memory T Cells in Autoimmune Diseases. *Mol. Pharmacol.* **2005**, *68*, 1254–1270, doi:10.1124/mol.105.015669.
12. Schmalhofer, W.A.; Bao, J.; McManus, O.B.; Green, B.; Matyskiela, M.; Wunderler, D.; Bugianesi, R.M.; Felix, J.P.; Hanner, M.; Linde-Arias, A.-R.; et al. Identification of a New Class of Inhibitors of the Voltage-Gated Potassium Channel, K v 1.3, with Immunosuppressant Properties †. *Biochemistry* **2002**, *41*, 7781–7794, doi:10.1021/bi025722c.
13. Ren, Y.R.; Pan, F.; Parvez, S.; Fleig, A.; Chong, C.R.; Xu, J.; Dang, Y.; Zhang, J.; Jiang, H.; Penner, R.; et al. Clofazimine Inhibits Human Kv1.3 Potassium Channel by Perturbing Calcium Oscillation in T Lymphocytes. *PLoS ONE* **2008**, *3*, e4009, doi:10.1371/journal.pone.0004009.
14. Chandy, K.G.; Norton, R.S. Peptide Blockers of Kv1.3 Channels in T Cells as Therapeutics for Autoimmune Disease. *Curr. Opin. Chem. Biol.* **2017**, *38*, 97–107, doi:10.1016/j.cbpa.2017.02.015.
15. Chen, R.; Robinson, A.; Gordon, D.; Chung, S.-H. Modeling the Binding of Three Toxins to the Voltage-Gated Potassium Channel (Kv1.3). *Biophys. J.* **2011**, *101*, 2652–2660, doi:10.1016/j.bpj.2011.10.029.
16. Liu, S.; Zhao, Y.; Dong, H.; Xiao, L.; Zhang, Y.; Yang, Y.; Ong, S.T.; Chandy, K.G.; Zhang, L.; Tian, C. Structures of Wild-Type and H451N Mutant Human Lymphocyte Potassium Channel KV1.3. *Cell Discov.* **2021**, *7*, 1–5, doi:10.1038/s41421-021-00269-y.
17. Tyagi, A.; Ahmed, T.; Jian, S.; Bajaj, S.; Ong, S.T.; Goay, S.S.M.; Zhao, Y.; Vorobyov, I.; Tian, C.; Chandy, K.G.; et al. Rearrangement of a Unique Kv1.3 Selectivity Filter Conformation upon Binding of a Drug. *Proc. Natl. Acad. Sci.* **2022**, *119*, e2113536119, doi:10.1073/pnas.2113536119.
18. Leanza, L.; Henry, B.; Sassi, N.; Zoratti, M.; Chandy, K.G.; Gulbins, E.; Szabò, I. Inhibitors of Mitochondrial Kv1.3 Channels Induce Bax/Bak-Independent Death of Cancer Cells. *EMBO Mol. Med.* **2012**, *4*, 577–593, doi:10.1002/emmm.201200235.
19. Zaccagnino, A.; Managò, A.; Leanza, L.; Gontarewitz, A.; Linder, B.; Azzolini, M.; Biasutto, L.; Zoratti, M.; Peruzzo, R.; Legler, K.; et al. Tumor-Reducing Effect of the Clinically Used Drug Clofazimine in a SCID Mouse Model of Pancreatic Ductal Adenocarcinoma. *Oncotarget* **2017**, *8*, 38276–38293, doi:10.18632/oncotarget.11299.
20. Leanza, L.; Trentin, L.; Becker, K.A.; Frezzato, F.; Zoratti, M.; Semenzato, G.; Gulbins, E.; Szabo, I. Clofazimine, Psora-4 and PAP-1, Inhibitors of the Potassium Channel Kv1.3, as a New and Selective Therapeutic Strategy in Chronic Lymphocytic Leukemia. *Leukemia* **2013**, *27*, 1782–1785, doi:10.1038/leu.2013.56.
21. Hendrickx, L.A.; Dobričić, V.; Toplak, Ž.; Peigneur, S.; Mašič, L.P.; Tomašič, T.; Tytgat, J. Design and Characterization of a Novel Structural Class of Kv1.3 Inhibitors. *Bioorganic Chem.* **2020**, *98*, 103746, doi:10.1016/j.bioorg.2020.103746.
22. Wolber, G.; Langer, T. LigandScout: 3-D Pharmacophores Derived from Protein-Bound Ligands and Their Use as Virtual Screening Filters. *J. Chem. Inf. Model.* **2005**, *45*, 160–169, doi:10.1021/ci049885e.
23. Poli, G.; Seidel, T.; Langer, T. Conformational Sampling of Small Molecules With ICon: Performance Assessment in Comparison With OMEGA. *Front. Chem.* **2018**, *6*.

24. LigandScout v.4.4 Available from Inte:Ligand. Https://Www.Inteligand.Com/Ligandscout.
25. Lacerda, A.E.; Kramer, J.; Shen, K.-Z.; Thomas, D.; Brown, A.M. Comparison of Block among Cloned Cardiac Potassium Channels by Non-Antiarrhythmic Drugs. *Eur. Heart J. Suppl.* **2001**, *3*, K23–K30, doi:10.1016/S1520-765X(01)90003-3.
26. Leanza, L.; Romio, M.; Becker, K.A.; Azzolini, M.; Trentin, L.; Managò, A.; Venturini, E.; Zaccagnino, A.; Mattarei, A.; Carraretto, L.; et al. Direct Pharmacological Targeting of a Mitochondrial Ion Channel Selectively Kills Tumor Cells In Vivo. *Cancer Cell* **2017**, *31*, 516-531.e10, doi:10.1016/j.ccell.2017.03.003.
27. Peruzzo, R.; Mattarei, A.; Romio, M.; Paradisi, C.; Zoratti, M.; Szabò, I.; Leanza, L. Regulation of Proliferation by a Mitochondrial Potassium Channel in Pancreatic Ductal Adenocarcinoma Cells. *Front. Oncol.* **2017**, *7*, 239, doi:10.3389/fonc.2017.00239.